Synthesis and Simulation of CaF$_2$@Al(OH)$_3$ Core-Shell Coated Solid Lubricant Composite Powder

Zhaoqiang Chen [1,2,*], Niansheng Guo [1,2], Chonghai Xu [1,2], Lianggang Ji [1,2], Runxin Guo [1,2] and Benyuan Wang [1,2]

[1] School of Mechanical and Automotive Engineering, Qilu University of Technology (Shandong Academy of Sciences), Jinan 250353, China; G1758251323@163.com (N.G.); xch@qlu.edu.cn (C.X.); jilianggang123@126.com (L.J.); guorunxin163@163.com (R.G.); wangbenyuan1994@163.com (B.W.)
[2] Key Laboratory of Advanced Manufacturing and Measurement and Control Technology for Light Industry in Universities of Shandong, Qilu University of Technology (Shandong Academy of Sciences), Jinan 250353, China
[*] Correspondence: czq@qlu.edu.cn

Abstract: In self-lubricating ceramic tools, adding CaF$_2$ will significantly reduce the mechanical properties of ceramic tools. Based on heterogeneous nucleation theory, we have recently prepared aluminum hydroxide (Al(OH)$_3$) coating on calcium fluoride (CaF$_2$) through a liquid-phase heterogeneous nucleation method. By adding CaF$_2$@Al(OH)$_3$ coated powder to replace CaF$_2$ powder, the self-lubricating ceramic tools maintain higher lubricity while also having better mechanical properties. The coating process was further confirmed by using scanning electron microscopy (SEM) and transmission electron microscopy (TEM). In addition, we used the molecular simulation software to simulate the suspension system of CaF$_2$, Al(NO$_3$)$_3$·9H$_2$O, and Al(OH)$_3$ to study the process of Al(OH)$_3$ coating on the surface of CaF$_2$ particle to form CaF$_2$@Al(OH)$_3$ powders with core-shell structure. Further, the formation and evolution of Al(OH)$_3$ molecules on the surface of CaF$_2$ were analyzed.

Keywords: simulation; Al(OH)$_3$ coated CaF$_2$; solid lubricant; self-lubricating ceramic tool

1. Introduction

Preparing self-lubricating ceramic tools by adding solid lubricant to a ceramic matrix is an effective way to improve the performance of dry cutting tools [1,2]. As a high-temperature solid lubricant, calcium fluoride (CaF$_2$) is easy to combine with the substrate and the coating process is simple because it does not react with the ceramic material matrix during the sintering process, and it has good lubrication performance at high temperatures [3,4]. CaF$_2$ is a common solid lubrication in self-lubricating ceramic tools. However, due to the inherent characteristics of solid lubricants with weak mechanical properties, the addition of solid lubricants definitely reduce the mechanical properties of the ceramic tool matrix.

Powder surface coating can significantly improve the properties of composite materials and endow them with new functions through coating [5–11]. Through surface coating, the molecular scale preparation between particles in different phases of the composite powder can be realized, and the physical and chemical properties of the material are effectively improved [12–18]. At present, core-shell composite powders prepared via the surface coating method has been widely used in the preparation of ceramics and cemented carbide [19–22]. In recent years, some studies have introduced the surface coating methods of self-lubricating materials, which improves the mechanical and lubricating properties of the material, as well as opens up a new technical way for researching solid self-lubricating materials.

Wu et al. [23] synthesized core-shell structured h-BN@Ni powders via the electroless plating technique using hydrazine hydrate as a reducing agent. The addition of h-BN@Ni powders improved the microstructure of the self-lubricating ceramic tool and greatly improved the mechanical properties of the tool. Chen et al. [24] prepared core-shell structured (h-BN)/SiO_2 composite powders to improve the mechanical property of h-BN. Compared with the self-lubricating ceramic tool without (h-BN)/SiO_2 composite powders, the mechanical properties of the self-lubricating ceramic tool with (h-BN)/SiO_2 composite powders were greatly improved.

In the present study, Aluminum hydroxide coated calcium fluoride composite powders (CaF_2@$Al(OH)_3$) were synthesized via the liquid-phase heterogeneous nucleation method. The composite particles had a core-shell structure. Molecular simulation software was used to simulate the suspension system of CaF_2, $Al(NO_3)\cdot9H_2O$, and aluminum hydroxide ($Al(OH)_3$) to study the process of $Al(OH)_3$ coating on the surface of CaF_2 particles to form CaF_2@$Al(OH)_3$ powders with core-shell structure. The formation and evolution of $Al(OH)_3$ molecules on the surface of CaF_2 were analyzed. The coating process was further confirmed by using scanning electron microscopy (SEM) and transmission electron microscopy (TEM).

2. Experimental Procedure

2.1. Materials and Processing

The starting powders used to fabricate the CaF_2@$Al(OH)_3$ coated particles were commercially available $Al(NO_3)_3\cdot9H_2O$ (purity > 99.9%, Shanghai Fine Chemical Co., Ltd., Shanghai, China), sodium acetate (analytically pure, Tianjin Chemical Reagent Factory, China), CaF_2 (purity > 99.9%, Shanghai Chaowei Nanomaterials Science and Technology Co., Ltd., China), aqueous ammonia, and absolute ethanol were used as received without further purification.

2.2. Synthesis of CaF₂@Al(OH)₃ Powders

Firstly, CaF_2 powder was pretreated via acid washing. Treated CaF_2 was washed with distilled water until the supernatant was weakly acidic. Then, distilled water was added to CaF_2 powder to prepare a dilute suspension with a concentration of 0.1 mol/L. Polyethylene glycol was used as a dispersant and then polyethylene glycol was added to the prepared suspension to be fully stirred, ultrasonically dispersed for 30 min.

Next, 0.1–0.2 mol/L $Al(NO_3)_3\cdot9H_2O$ (analytical pure) solution was added to the fully stirred suspension. Then, a buffer solution prepared via sodium acetate (analytically pure) was added and used to carry out ultrasonic dispersion on the mixed suspension for 20 min.

The suspension was heated and rapidly stirred in DF-101S heat-collecting thermostatic heating magnetic stirrer. After heating to 65–85 °C, aqueous ammonia was added dropwise at a speed of 1–6 mL/min to increase the pH value of the suspension. After the pH value reached 6.5–8.5, the suspension was kept warm for 30 min to fully carry out the reaction. The obtained $Al(OH)_3$ was uniformly coated on the surface of CaF_2 particles in the form of precipitates.

The suspension was placed for 2 h and centrifuged at 6000 r/min in a high-speed centrifuge. Then, the suspension was repeatedly washed with absolute ethanol to prevent agglomeration of the CaF_2@$Al(OH)_3$ composite powder. The washed composite powder was dried in a vacuum at 110 °C for 24 h to obtain CaF_2@$Al(OH)_3$ core-shell coated composite powder.

2.3. Sample Characterization

The morphologies and microstructures were tested and analyzed using a field-emission scanning electron microscope (SEM, SUPRA^{TM} 55, Carl Zeiss Group, Oberkochen, Germany) and a transmission electron microscope (TEM, JEM-1400, JEOL, Tokyo, Japan).

3. Results and Discussion

3.1. Simulation of Adsorption of Al(OH)$_3$ Molecules on CaF$_2$ Surface

According to the aforementioned precipitation conditions of Al(OH)$_3$ crystals, Al(OH)$_3$ molecules are drawn using Material Studio software, in which the crystal cell model of CaF$_2$ in the system was established. The obtained crystal cell model of Al(OH)$_3$ molecules and CaF$_2$ is shown in Figure 1.
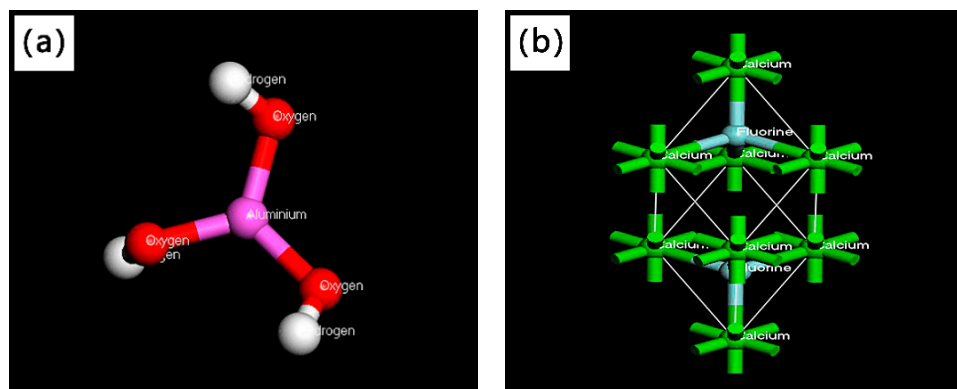

Figure 1. Model: (**a**) aluminum hydroxide (Al(OH)$_3$) molecular model; (**b**) calcium fluoride (CaF$_2$) unit cell model.

Molecular dynamics are used to simulate the adsorption of Al(OH)$_3$ molecules without fixing the atoms on the surface of CaF$_2$. The pH value of the system is set to 7.5, the reaction temperature is 75 °C, and the concentration of aluminum ions in the solution is 0.15 mol/mL. The simulation process and results are as follows.

Select CaF$_2$ protocell section (1 0 0) set the layer thickness to 2. A vacuum layer with a thickness of 20 A is built and the whole above is used as an adsorption template, in which Al(OH)$_3$ molecules are used as adsorbents. In the initial state, the system model is shown in Figure 2a. The system of CaF$_2$ in the cell is fixed. Al(OH)$_3$ molecules are placed in any position in the vacuum layer and universal is selected as the force field. The energy of surface atoms and molecules are calculated by the geometry optimization function in the software Forcite module. At this time, Al(OH)$_3$ molecules are adsorbed spontaneously to the surface of CaF$_2$ particles in order to reduce the energy of the system. However, due to the CaF$_2$ surface being fixed, Al(OH)$_3$ molecules can only adsorb on the surface of CaF$_2$. The system simulation results are shown in Figure 2b.
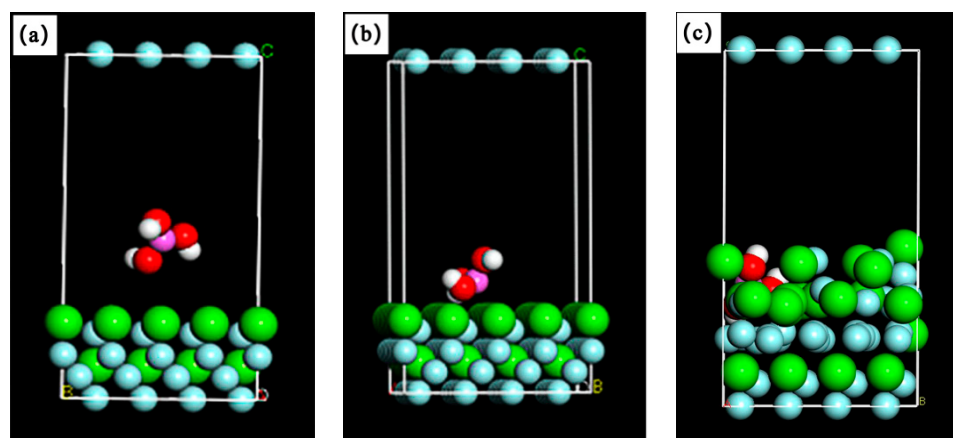

Figure 2. Adsorption process of Al(OH)$_3$ molecules on the CaF$_2$ surface: (**a**) before adsorption; (**b**) the surface is attached; and (**c**) fully adsorbed.

After the CaF_2 cell is decoupled, the above operation is repeated and simulated. The simulation results are shown in Figure 2c. It can be seen from the figure that CaF_2 molecules interact with $Al(OH)_3$ molecules and the aluminum oxide molecules have established a stable adsorption relationship with CaF_2 molecules.

The energy change of the above adsorption process system is shown in Figure 3. It can be seen from Figure 3a that the entropy of the system is continuously reduced until the stabilization of the $Al(OH)_3$ molecule on the CaF_2 surface is less than zero, from 29 kcal/mol stable in −5 kcal/mol, indicating that the system gradually becomes an orderly state. The above calculation shows that the reaction of the $Al(OH)_3$ molecule to the CaF_2 surface is a spontaneous reaction. It can be seen from Figure 3b that the entropy of the system is from 650 kcal/mol at the beginning to −33.681704 kcal/mol when the $Al(OH)_3$ molecule interacts with the surface of the CaF_2 cell after the CaF_2 cell is removed.
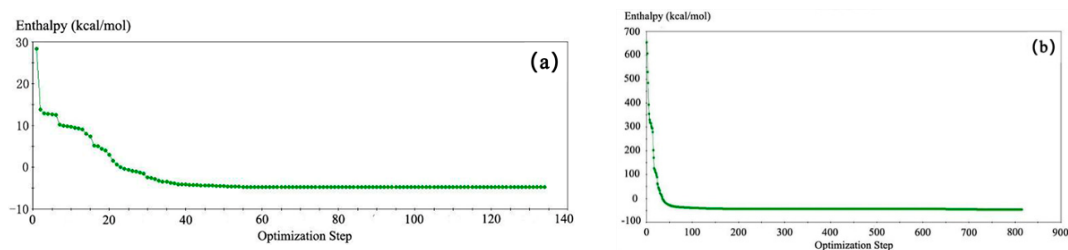

Figure 3. Change of entropy of adsorption process: (**a**) the change of the entropy value in the fixed surface atomic operation; (**b**) the entropy change in the operation when the surface atoms are not constrained.

Compared with the entropy change in the surface atomic operation of the fixed surface, the energy conversion of the CaF_2 cell is more intense and the reaction time is shorter, which indicates that the reaction driving force of the CaF_2 cell is more stable than that of Figure 3a,b. Thus, the interface after adsorption will be more stable. Compared with the previous reaction, the entropy change of the system is gradually reduced.

Using the energy unit in the Forcite module of the Materials Studio software, the total energy of the adsorbed system is calculated. The formula is:

$$E_b = E_T - (E_S + E_M) \tag{1}$$

where E_b is the binding energy of the adsorption interface, E_T is the total energy of the system, E_S is the total surface energy of the system, and E_M is the total molecular energy of each molecule.

The corresponding values can be calculated $E_T = -4.754992 \, kcal/mol$, $E_S = 0.000000 \, kcal/mol$, $E_M = 28.926712 \, kcal/mol$, the above results are substituted into the formula (1) can be obtained:

$$E_b = -4.754992 - 0.000000 - 28.926712 = -33.681704 \, kcal/mol \tag{2}$$

The coating process of $Al(OH)_3$ on the CaF_2 surface is a process in which $Al(OH)_3$ molecules gradually adsorb to CaF_2 solid surface. If the Gibbs system is negative, indicating that the reaction is exothermic, then the adsorption is stable and crystallization will occur spontaneously. If the adsorption energy is positive, indicating that the adsorption process is endothermic, then the adsorption is unstable and crystallization cannot occur spontaneously. In the above MS calculation of the CaF_2-$Al(OH)_3$ system, the adsorption energy is found to be negative, indicating that the system after adsorption is thermodynamically stable, meaning the system can realize spontaneous and stable adsorption. Therefore, $Al(OH)_3$ can be stably adsorbed on the surface of CaF_2. The test results show that the simulation results are consistent with the test results.

3.2. Simulation of Suspension Adsorption Interface

The molecular dynamics simulation is carried out using the Forcite module of Material Studio software. Set the system pH value to 7.5, the reaction temperature is 75 °C, and the concentration of $Al(OH)_3$ in the solution is 0.15 mol/mL. The simulation process and the results were as follows.

First, a CaF_2 crystal cell cross section was established in which the unit cell was connected with the aqueous solution containing $Al(OH)_3$ in a layered manner to simulate the adsorption of $Al(OH)_3$ in the solution. The force field is the compass and the molecular dynamics of Materials Studio software is used to simulate the motion of $Al(OH)_3$ and the combination of CaF_2. The primary cell cross section (1 1 0) of CaF_2 is selected and the thickness is set to 3 to establish the layer of CaF_2, as shown in Figure 4a. At the same time, a model of colloidal hydrate of 0.15 mol/mL $Al(OH)_3$ is established in the system, as shown in Figure 4b.
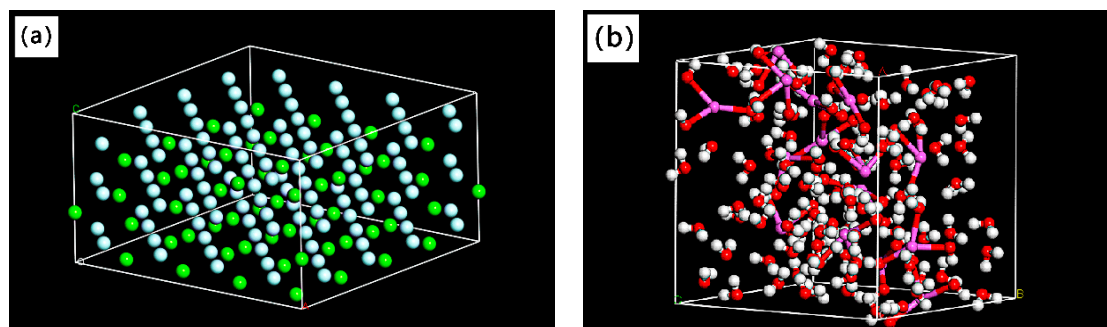

Figure 4. Model: (**a**) the model of CaF_2 surface; (**b**) the model of an aqueous solution containing $Al(OH)_3$ molecules.

In the operation process, the two models are linked and subjected to kinetic calculations. The results of the adsorption of $Al(OH)_3$ molecules into the CaF_2 cells can be obtained as shown in Figure 5a,b. A large number of $Al(OH)_3$ molecules adsorbed on the surface of CaF_2 and separated from the H_2O molecules lead to a solution layered and adsorbed with $Al(OH)_3$ that forms a precipitate with CaF_2 and has a density field analysis of $Al(OH)_3$-CaF_2, with a suspension system created by the density field module, shows that the density field of the suspension system is clearly separated due to the formation of different substances in the system. The structure is that the top layer is the H_2O layer, the middle layer is the $Al(OH)_3$ and CaF_2 binder layer, and the bottom layer is the CaF_2 layer, as shown in Figure 5c.
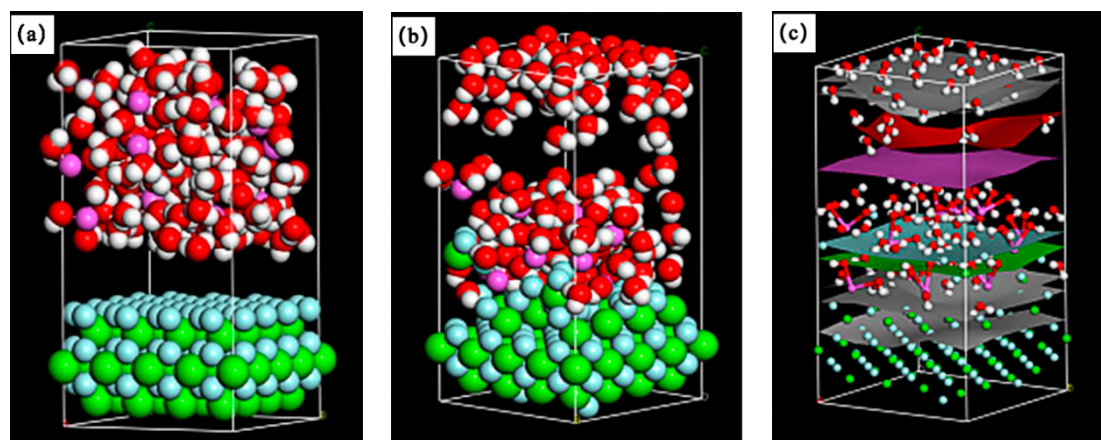

Figure 5. $Al(OH)_3$-CaF_2 suspension adsorption process: (**a**) before adsorption; (**b**) fully adsorbed; and (**c**) the density field analysis of the system.

Figure 6 shows the change in the energy of the CaF_2-$Al(OH)_3$ suspension system during the simulation. It can be seen from Figure 6 that until the end of the entire process, the potential energy in the system, the interface separation energy, and the total energy are finally converged to their respective stable and negative values. Further, the total kinetic energy in the system is stabilized, which indicates that the $Al(OH)_3$ molecule has been stopped after the reaction of the system, i.e., the system has established a stable adsorption relationship. The above calculation further confirms that $Al(OH)_3$ colloidal molecules can be stably coated on CaF_2 surface under the experimental conditions setup in this subject.
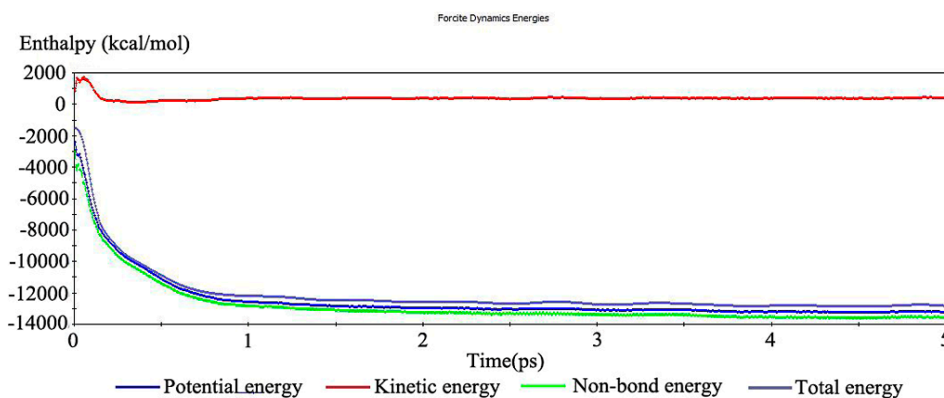

Figure 6. Energy change process of the CaF_2-$Al(OH)_3$ suspension system.

The simulation experiment and calculation of the above coating process shows that $Al(OH)_3$ colloid molecules can stably adsorb on the surface of CaF_2 under the set test conditions. Further, it establishes a stable adsorption interface by forming new chemical bonds, which thus form a core-shell coated with a $CaF_2@Al(OH)_3$ composite powder. This simulation provides good technical support for the preparation experiment of core-shell coated $CaF_2@Al(OH)_3$ composite powder. Our experiments also prove that the core-shell coated $CaF_2@Al(OH)_3$ composite powder had good performance.

3.3. Test Analysis

Figure 7a,b show SEM photographs of the pre-coated CaF_2 powder and the coated $CaF_2@Al(OH)_3$ composite powder. The surface morphology of each powder particle is visually shown.

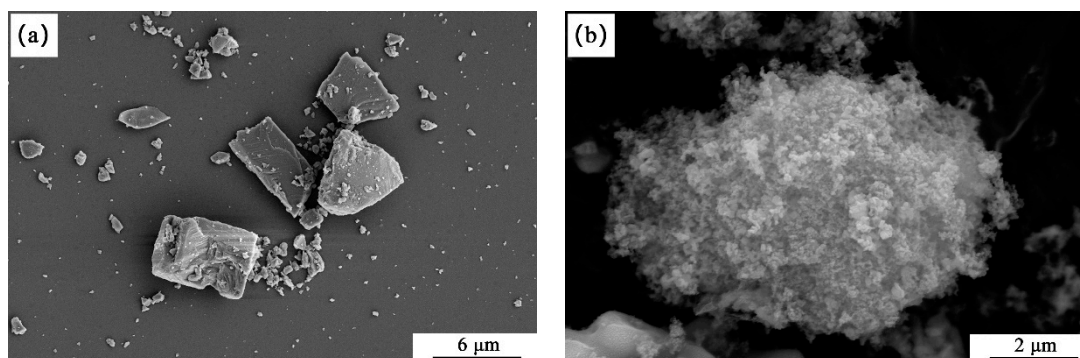**Figure 7.** Scanning electron microscope (SEM) morphology: (**a**) CaF_2 powders; (**b**) $CaF_2@Al(OH)_3$ composite powder.

It can be seen from Figure 7 that the morphology of CaF_2 is very different from that of CaF_2 before coating. The surface of CaF_2 in Figure 7a is obvious and its surface is not very flat. It is clear that the coated CaF_2 surface is coated with a layer of granular material $Al(OH)_3$, forming a uniform and dense coating.

Figure 8 shows TEM photographs of the above coated microparticles. Figure 8a is a transmission electron micrograph of uncoated CaF_2; Figure 8b is a transmission electron micrograph of coated $CaF_2@Al(OH)_3$ coated microparticles. As can be seen when comparing the two figures, after CaF_2 was coated with $Al(OH)_3$, its morphology changed greatly. Figure 8a shows that the uncoated CaF_2 is flake and it can be seen from Figure 8b that the surface of CaF_2 is coated with an $Al(OH)_3$ layer with a thickness of about 50–200 nm. $Al(OH)_3$ is evenly coated on the surface of calcium fluoride to form a core-shell structure and the coating effect is good.
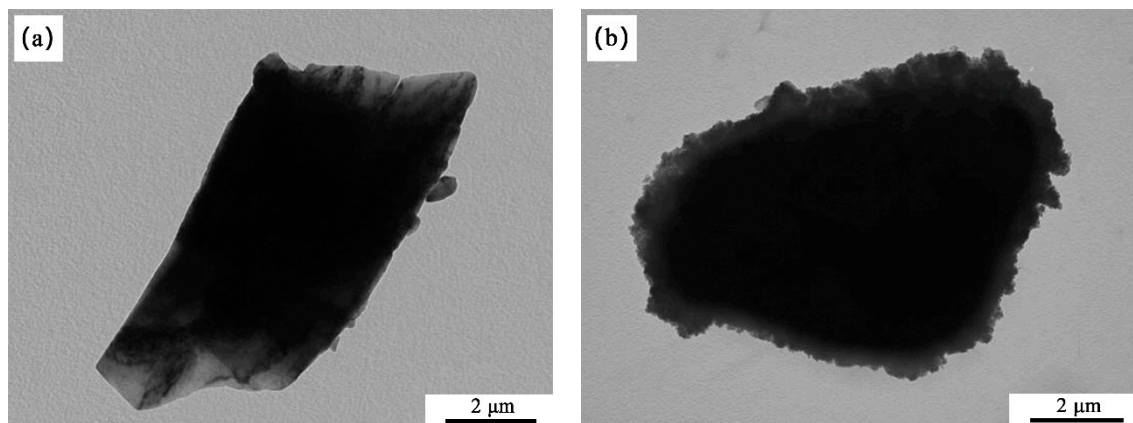

Figure 8. Transmission electron microscope (TEM) photographs: (**a**) CaF_2 powder; (**b**) $CaF_2@Al(OH)_3$ composite powders.

Based on the above analysis, $Al(OH)_3$ can be successfully coated on the surface of CaF_2. Based on the principle of nonuniform nucleation, $Al(OH)_3$ forms a dense and uniform coating layer. The cladding layer is deposited and connected with $Al(OH)_3$ particles and the effect of the coating is better.

4. Conclusion

Through the above simulation, it is verified that aluminum hydroxide can be coated on the surface of calcium fluoride, wherein the optimal coating process is determined. Experiments were carried out according to the simulation process. The results show that $Al(OH)_3$ can be stably adsorbed on the surface of CaF_2 under the experimental conditions. The stable adsorption interface can be formed by the interaction of CaF_2 and $Al(OH)_3$. The well-behaved core-shell structure of $CaF_2@Al(OH)_3$ coated particles was prepared. The following conclusions were obtained.

1. The formation process and energy change of $CaF_2@Al(OH)_3$ coated composite powder were simulated using Material Studio. It was verified that under experimental conditions, $Al(OH)_3$ colloidal molecules were stably adsorbed on the surface of CaF_2 and a stable adsorption interface was established through the formation of new chemical bonds. This formed a core-shell coated $CaF_2@Al(OH)_3$ composite powder. The simulation results are in good agreement with the theoretical calculation and experimental results.

2. The preparation process of $CaF_2@Al(OH)_3$ core-shell coated composite powder was designed. The prepared $CaF_2@Al(OH)_3$ and $CaF_2@Al_2O_3$ core-shell coated composite powders were characterized and analyzed using SEM and TEM, which proved that the coated particles formed the core-shell structure morphology.

Conflicts of Interest: The authors declare no conflict of interest.

References

1. Gajrani, K.K.; Sankar, M.R.; Dixit, U.S. Environmentally friendly machining with MoS_2-filled mechanically microtextured cutting tools. *J. Mech. Sci. Technol.* **2018**, *32*, 3797–3805. [CrossRef]
2. Xing, Y.; Deng, J.; Wu, Z.; Liu, L.; Huang, P.; Jiao, A. Analysis of tool-chip interface characteristics of self-lubricating tools with nanotextures and WS_2/Zr coatings in dry cutting. *Int. J. Adv. Manuf. Technol.* **2018**, *97*, 1637–1647. [CrossRef]
3. Deng, J.; Yang, X.; Liu, J. Self-lubricating behaviours of ceramic tools in dry cutting. *Int. J. Mach. Mach. Mater.* **2006**, *1*, 213–222.
4. Xu, C.; Xiao, G.; Zhang, Y.; Fang, B. Finite element design and fabrication of $Al_2O_3/TiC/CaF_2$ gradient self-lubricating ceramic tool material. *Ceram. Int.* **2014**, *40*, 10971–10983. [CrossRef]
5. Razavi, M.; Fathi, M.; Savabi, O.; Razavi, S.M.; Heidari, F.; Manshaei, M.; Vashaeef, D.; Tayebi, L. In vivo study of nanostructured diopside ($CaMgSi_2O_6$) coating on magnesium alloy as biodegradable orthopedic implants. *Appl. Surf. Sci.* **2014**, *313*, 60–66. [CrossRef]
6. Wu, Q. Applicatin of Modification Technology on Surface Coating to Ceramic Process. *Adv. Ceram.* **2000**, *4*. [CrossRef]
7. Takahashi, N.; Hashimoto, S.; Daiko, Y.; Honda, S.; Iwamoto, Y. High-temperature shrinkage suppression in refractory ceramic fiber board using novel surface coating agent. *Ceram. Int.* **2018**, *44*, 16725–16731. [CrossRef]
8. Weng, B.; Yang, M.Q.; Zhang, N.; Xu, Y.J. Toward the enhanced photoactivity and photostability of ZnO nanospheres via intimate surface coating with reduced graphene oxide. *J. Mater. Chem. A* **2014**, *2*, 9380–9389. [CrossRef]
9. Say, Y.; Aksakal, B.; Dikici, B. Effect of hydroxyapatite/SiO_2, hybride coatings on surface morphology and corrosion resistance of REX-734 alloy. *Ceram. Int.* **2016**, *42*, 10151–10158. [CrossRef]
10. Yuan, Y.; Li, Z. Microstructure and Tribology Behaviors of In-situ WC/Fe Carbide Coating Fabricated by Plasma Transferred Arc Metallurgic Reaction. *Appl. Surf. Sci.* **2017**, *423*, 13–24. [CrossRef]
11. Zhou, W.; Zhou, K.; Li, Y.; Deng, C.; Zeng, K. High temperature wear performance of HVOF-sprayed Cr_3C_2-WC-NiCoCrMo and Cr_3C_2-NiCr hardmetal coatings. *Appl. Surf. Sci.* **2017**, *416*, 33–44. [CrossRef]
12. Sahan, H.; Göktepe, H.; Patat, S. A Novel Method to Improve the Electrochemical Performance of $LiMn_2O_4$ Cathode Active Material by $CaCO_3$ Surface Coating. *J. Mater. Sci. Technol.* **2011**, *27*, 415–420. [CrossRef]
13. Liu, Z.; Miyauchi, M.; Uemura, Y.; Cui, Y.; Hara, K.; Zhao, Z.; Sunahara, K.; Furube, A. Enhancing the performance of quantum dots sensitized solar cell by SiO_2 surface coating. *Appl. Phys. Lett.* **2010**, *96*, 3183. [CrossRef]
14. Shen-Wei, X.U.; Jiang, L.; Huang, X.Z.; Xu, S.; Jiang, L.; Huang, X.; Du, Z.; Xiao, L. Silicon Carbide Doped Beryllium Foam Ceramic Preparation by the Surface of Polyurethane Coating. *Surf. Technol.* **2016**. [CrossRef]
15. Sebben, J.; Canevese, V.A.; Alessandretti, R.; Pereira, G.K.; Sarkis-Onofre, R.; Bacchi, A.; Spazzin, A.O. Effect of Surface Coating on Bond Strength between Etched Feldspar Ceramic and Resin-Based Luting Agents. *BioMed Res. Int.* **2018**, *2018*, 3039251. [CrossRef]
16. Wang, J.; Huang, S.; He, M.; Wangyang, P.; Lu, Y.; Huang, H.; Xu, L. Microstructural characteristic, outward-inward growth behavior and formation mechanism of MAO ceramic coating on the surface of ADC12 Al alloy with micro-groove. *Ceram. Int.* **2018**, *44*, 7656–7662. [CrossRef]
17. Grigoriev, S.N.; Vereschaka, A.A.; Vereschaka, A.S.; Kutin, A.A. Cutting Tools Made of Layered Composite Ceramics with Nano-Scale Multilayered Coatings. *Procedia CIRP* **2012**, *1*, 301–306. [CrossRef]
18. He, G.; Deng, X.; Cen, Y.K.; Li, X.Y.; Luo, E.; Nie, R.R.; Zhao, Y.; Liang, Z.H.; Chen, Z.Q. Development and Characterization of Nano-TiO2/HA Composite Bioceramic Coating on Titanium Surface. *Key Eng. Mater.* **2007**, *336–338*, 1802–1805. [CrossRef]
19. Nazemosadat, S.M.; Foroozmehr, E.; Badrossamay, M. Preparation of Alumina/Polystyrene Core-Shell Composite Powder via Phase Inversion process for Indirect Selective Laser Sintering Applications. *Ceram. Int.* **2018**, *44*, 596–604. [CrossRef]
20. Lin, J.F.; Cao, S.H.; Huang, Q.F. Preparation of Co/Fe Core-shell composite powder by chemical plating. *Mater. Sci. Eng. Powder Metall.* **2010**, *15*, 265–270.

21. Luo, X.T.; Li, C.X.; Shang, F.L.; Yang, G.J.; Wang, Y.Y.; Li, C.J. WC-Co Composite Coating Deposited by Cold Spraying of a Core-Shell-Structured WC-Co Powder. *J. Therm. Spray Technol.* **2015**, *24*, 100–107. [CrossRef]

22. Hu, Y.; Xu, C.; Xiao, G.; Yi, M.; Chen, Z.; Zhang, J. Electrostatic Self-assembly Preparation of Reduced Graphene Oxide-Encapsulated Alumina Nanoparticles with Enhanced Mechanical Properties of Alumina Nanocomposites. *J. Eur. Ceram. Soc.* **2018**, *38*, 5122–5133. [CrossRef]

23. Wu, G.; Xu, C.; Xiao, G.; Yi, M.; Chen, Z.; Chen, H. An advanced self-lubricating ceramic composite with the addition of core-shell structured h-BN@Ni powders. *Int. J. Refract. Met. Hard Mater.* **2018**, *72*, 276–285. [CrossRef]

24. Chen, H.; Xu, C.; Xiao, G.; Chen, Z.; Ma, J.; Wu, G. Synthesis of (h-BN)/SiO_2 core–shell powder for improved self-lubricating ceramic composites. *Ceram. Int.* **2016**, *42*, 5504–5511. [CrossRef]